PERGAMON

International Journal of Solids and Structures 40 (2003) 5441–5454

INTERNATIONAL JOURNAL OF SOLIDS and STRUCTURES

www.elsevier.com/locate/ijsolstr

Modelling paper as a two-dimensional elastic–plastic stochastic network

C.A. Bronkhorst *

Weyerhaeuser Company, Federal Way, WA 98063-9777, USA

Received 26 June 2002; received in revised form 17 April 2003

Abstract

Stochastic two-dimensional elastic–plastic network models are used to represent the inelastic deformation behavior of well-bonded paper. Linear kinematic hardening is employed with an initial non-zero back stress to represent anisotropic fiber yield. Network models are used to simulate simple monotonic tension and simple cyclic tension of paper materials. The performance of the models is compared to experimental results and found to perform reasonably well. The results suggest that interfiber bonding must be explicitly accounted for to adequately describe the material. Some discrepancy between the model and experimental cyclic tension results is believed to be due to time-dependent strain recovery in the material which is not represented in the network models. Experimental results are also presented which show that simple tension failure in these materials occurs along a line of localized deformation in a majority of the samples. This line is generally observed to form immediately prior to failure and is oriented at a well-defined angle with respect to the loading direction.

Keywords: Paper; Stochastic; Network; Tension; Cyclic; Inelastic; Failure zone; Stress distribution

1. Introduction

Paper is a multi-scale composite material. It is constructed in the wet state from discrete tubular fibers which are bound to each other primarily through hydrogen bonds (Retulainen et al., 1998). The planar distribution of fiber centers is in general non-uniform. The orientation distribution of the fibers is generally weighted in the direction of manufacturing, resulting in an anisotropic material. A micrograph image of the surface of laboratory made material used for this study is given in Fig. 1. The fibers themselves are also a composite material with three significant layers comprising its wall and in each layer there exist largely crystalline cellulose microfibrils embedded in a mixture of amorphous, cellulosic polymers. In each wall layer the microfibrils align themselves differently with respect to the fiber cylinder axis. Within each

* Present address: Los Alamos National Laboratory, Theoretical Division, T-3, P.O. Box 1663, Mail Stop B216, Los Alamos, NM 87545, USA. Tel.: +1-505-665-0122; fax: +1-505-665-5926.

E-mail address: cabronk@lanl.gov (C.A. Bronkhorst).

0020-7683/$ - see front matter © 2003 Elsevier Ltd. All rights reserved.
doi:10.1016/S0020-7683(03)00281-6

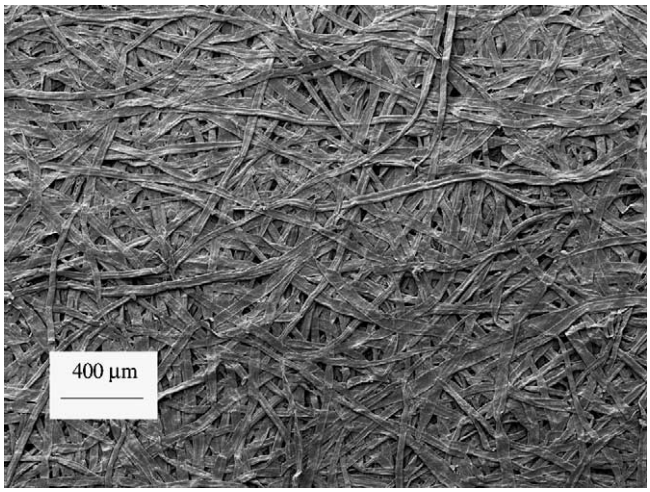

Fig. 1. Top view micrograph of a sample of uniform fiber orientation laboratory material used for the monotonic simple tension tests. Mean fiber width is 30 μm and mean fiber length is 2.2 mm.

population of fibers there are generally earlywood and latewood fiber types. The earlywood fibers (formed in the spring) are large in diameter with a thin wall whereas the latewood fibers (formed in the summer) are smaller in diameter and have a thicker wall. Because earlywood fibers are more easily collapsed they are better able to form interfiber bonds. Fibers are generally curled and kinked when consolidated in the sheet. Curlated fibers produce paper which has a lower in-plane Young's modulus and tensile strength. For each fiber or sheet property mentioned above, each variable is best defined by a distribution rather than a mean value. A recent review of wood pulp fibers is presented by Mark (2001).

In terms of mechanical properties, paper is an orthotropic material. It can be thought of as a high density disordered cellular solid. As such it is susceptible to both material and structural mechanisms of deformation and failure (Bronkhorst and Bennett, 2001). A portion of the amorphous polymers within the fibers are highly hygroscopic so their mechanical properties are highly sensitive to moisture content and temperature. Paper is also deformation rate sensitive. Given this complexity, little work has been done to develop macroscopic constitutive models for this class of material (Ramasubramanian and Wang, 1999). Only recently has a general three-dimensional phenomenological elastic–plastic representation of paper been developed (Xia et al., 2002).

From a micromechanical perspective, much work has been done spanning the size range between fiber and sheet for the elastic properties of paper (e.g. Cox, 1952; Van den Akker, 1962; Perkins and Mark, 1976; Ostoja-Starzewski and Stahl, 2000; Perkins, 2001). Much less has been done to quantify inelastic deformation. Ramasubramanian and Perkins (1988) defined the representative volume element (RVE) as a single fiber with fiber crossings and applied an affine deformation field to the element. Sinha and Perkins (1995) derived a two-dimensional incremental elastic–plastic constitutive model for paper based upon a homogenization of the deformation response of the single fiber with fiber crossings RVE. Wang (2000) applied the model of Sinha and Perkins (1995) to the problems of loading/unloading in simple tension and Mullen burst (roughly biaxial tension). Wang assumed that all plastic deformation occurred in the interfiber bond regions and that the process of unloading was completely elastic. The Mullen burst test was simulated but significant discrepancy existed between simulation and experimental results. The general approach of Ramasubramanian and Perkins (1988) does not allow study of larger size scale phenomena such as flocculation, multi-population mixtures, interfiber load sharing, and deformation localization. Although they

did not attempt to quantitatively describe experimental results, Räisänen et al. (1996) represented paper as a two-dimensional network with the fibers as isotropic elastic–plastic beams.

Here two-dimensional stochastic computational network models are used (similar to network models presented by Åström et al., 1994; Heyden and Gustafsson, 1998; Räisänen et al., 1996; Ostoja-Starzewski, 1998) to describe simple tension experimental results in an attempt to link the inelastic deformation behavior of the fiber to that of the planar material. We begin by outlining the numerical modelling procedure.

2. Computational network model

2.1. Network construction

Each network was derived from a marked two-dimensional random point field. The pseudo-random function RAND within the C library was used which compares reasonably well with the Poisson distribution for a large population,

$$p(r) = \frac{\bar{n}_{\mathrm{f}}^{r}}{r!}\exp(-\bar{n}_{\mathrm{f}}). \tag{1}$$

Eq. (1) represents the probability of finding r fiber centers per unit area for a network with a mean number of fiber centers per unit area of $\bar{n}_{\mathrm{f}}$. Each point is associated with a length (l_{f}) and orientation (θ). Generally, the length probability density function used for construction of the models is given by

$$p(l_{\mathrm{f}}) = \frac{(l_{\mathrm{f}}/b_1)^{b_2-1}}{b_1(b_2-1)!}\exp(-l_{\mathrm{f}}/b_1), \quad \bar{l}_{\mathrm{f}} = b_1 b_2, \tag{2}$$

where b_1 and b_2 are constants and $\bar{l}_{\mathrm{f}}$ is the mean fiber length. The orientation probability density function used is given by

$$p(\theta) = \frac{1}{\pi}(1 + a_1\cos 2\theta + a_2\cos 4\theta + \cdots + a_n\cos 2n\theta). \tag{3}$$

For the simulations presented here, the choice is made to begin simply, therefore only one fiber population was used, the fibers were assumed to be initially straight, fiber length was taken as constant, and $a_n = 0 \quad \forall n \geqslant 2$. Note that $a \in [0,1]$.

The center of each fiber was deposited onto a square of dimension $L + 2\bar{l}_{\mathrm{f}}$, a representative product of which is shown in Fig. 2. Network density ρ_n (kg/m^3), was determined from the product of mean areal coverage $\bar{c}$, and fiber wall density ρ_{f} (1540 kg/m^3).

$$\rho_n = \bar{c}\rho_{\mathrm{f}}, \tag{4}$$

$$\bar{c} = \frac{L_{\mathrm{f}} w_{\mathrm{f}}}{A_n}, \tag{5}$$

where L_{f} is the total fiber length within the boundaries of the network area $A_n = L \times L$ and w_{f} is the fiber width. Next, network connectivity was determined, non-load bearing fiber segments were removed and the network was trimmed to final dimension ($L \times L$). A representative network model is shown in Fig. 3. A network size of 10 mm $\times$ 10 mm was used for all the models discussed here. This size represents a balance between the appropriate selection of a RVE size and the available computational resources. The commercially available finite element code ABAQUS (1998) was used for the simulations.

A node was placed at each interfiber crossing and an initially straight Timoshenko beam element with five integration points across the width of the beam was assigned to each connected fiber segment. The mean

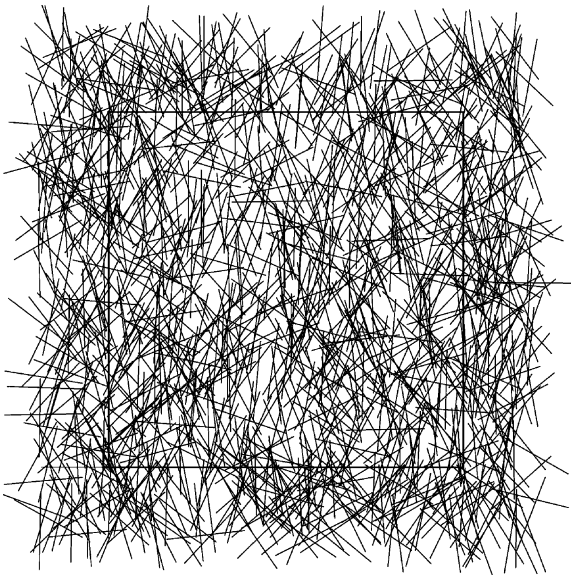

Fig. 2. A two-dimensional fiber network before trimming free fiber ends and edges of the square. The density of the network is 600 kg/m^3 and the fiber orientation parameter $a_1 = 0.79$. The length of the fibers is 2.2 mm and the size of the target square is 10 mm. Note that the width of the fibers is not drawn to scale.

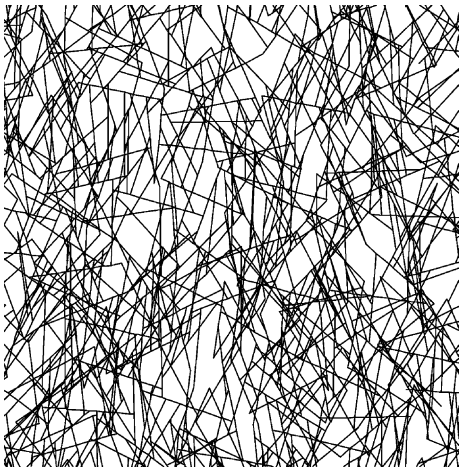

Fig. 3. The same two-dimensional fiber network as shown in Fig. 2 after trimming free fiber ends and edges. The size of the square is 10 mm. Note that the width of the fibers is not drawn to scale.

beam segment length for the simulations presented here was ~7 times the beam width. Each bond was rigid and plastic shear deformation was not accounted for. The elastic shear stress was independent from the yield stress calculation as per the current element formulation (ABAQUS, 1998). For simple tension considered here, multi-point constraint displacement boundary conditions were applied to the loaded edges. This forced the nodes along the loaded edges to remain on a line perpendicular to the loading direction while still allowing for lateral displacement. The nodes along the unloaded edges were unrestrained.

For two-dimensional models, the expected number of fiber crossings per unit network area for finite fiber lengths is given by the following relationship (Corte, 1971),

$$n_c = \frac{1}{2\pi}(1+\exp(-\bar{c}))\left(\frac{\bar{c}}{w_f}\right)^2\left(1-\frac{1}{6}a_1^2\right). \tag{6}$$

The expected two-dimensional mean distance between interfiber bonds along a fiber is given by (Deng and Dodson, 1994),

$$\bar{l}_{2D} = \frac{2\pi w_f}{\bar{c}(1+\exp(-\bar{c}))\left(1-\frac{1}{6}a_1^2\right)}. \tag{7}$$

For fibers of rectangular cross-section, the mean projected fiber crossing area within the network is given by (Perkins, 1980),

$$\overline{A}_c = \frac{w_f^2}{2\left(\frac{1}{\pi}-\frac{1}{6}a_1^2\right)}. \tag{8}$$

2.2. Fiber constitutive model

Although wood pulp fibers have a significant viscous component to their inelastic deformation behavior (Mark, 2001), it was decided to begin more simply by using an elastic–plastic constitutive model to represent the quasi-static deformation response of the fiber segments. The small-strain constitutive model with linear kinematic hardening is given below. Second and fourth rank tensors are denoted by single and double underscores respectively.

Strain rate,

$$\underline{\dot{\boldsymbol{\varepsilon}}} = \underline{\dot{\boldsymbol{\varepsilon}}}^e + \underline{\dot{\boldsymbol{\varepsilon}}}^p, \tag{9}$$

Cauchy stress rate,

$$\underline{\dot{\boldsymbol{\sigma}}} = \underline{\underline{\mathbf{L}}}\,\underline{\dot{\boldsymbol{\varepsilon}}}^e, \tag{10}$$

Isotropic elasticity,

$$\underline{\underline{\mathbf{L}}} = 2\mu\underline{\underline{\mathbf{I}}} + \left(\kappa - \frac{2}{3}\mu\right)\underline{\mathbf{1}}\otimes\underline{\mathbf{1}}, \tag{11}$$

Mises yield function,

$$F = f(\underline{\boldsymbol{\sigma}} - \underline{\boldsymbol{\alpha}}) - \sigma^0 = 0, \tag{12}$$

$$f(\underline{\boldsymbol{\sigma}} - \underline{\boldsymbol{\alpha}}) = \sqrt{\frac{3}{2}(\underline{\boldsymbol{\sigma}}' - \underline{\boldsymbol{\alpha}}')\cdot(\underline{\boldsymbol{\sigma}}' - \underline{\boldsymbol{\alpha}}')}, \tag{13}$$

$$\underline{\boldsymbol{\sigma}}' = \underline{\boldsymbol{\sigma}} - \frac{1}{3}\mathrm{tr}\,\underline{\boldsymbol{\sigma}}, \quad \underline{\boldsymbol{\alpha}}' = \underline{\boldsymbol{\alpha}} - \frac{1}{3}\mathrm{tr}\,\underline{\boldsymbol{\alpha}}, \tag{14}$$

Flow rule,

$$\underline{\dot{\boldsymbol{\varepsilon}}}^p = \dot{\bar{\varepsilon}}^p \frac{\partial F}{\partial \underline{\boldsymbol{\sigma}}}, \tag{15}$$

Kinematic hardening,

$$\dot{\underline{\boldsymbol{\alpha}}} = \frac{C}{\sigma^0}(\underline{\boldsymbol{\sigma}} - \underline{\boldsymbol{\alpha}})\dot{\bar{\varepsilon}}^{\mathrm{p}}, \quad \underline{\boldsymbol{\alpha}}^0 \neq \underline{\mathbf{0}}, \tag{16}$$

Equivalent plastic strain rate,

$$\dot{\bar{\varepsilon}}^{\mathrm{p}} = \sqrt{\frac{2}{3}\dot{\underline{\boldsymbol{\varepsilon}}}^{\mathrm{p}} \cdot \dot{\underline{\boldsymbol{\varepsilon}}}^{\mathrm{p}}}, \tag{17}$$

where μ and κ are shear and bulk moduli respectively, σ^0 is the initial yield stress, and C is a hardening constant. Note that in general an initial non-zero value was assigned to the back stress tensor to phenomenologically represent differential fiber behavior in tension and compression.

3. Experimental procedures

Commercially manufactured bleached wood pulp fibers made from the Kraft pulping process were used in their unrefined state to make laboratory materials. Both uniform and non-uniform fiber orientation sheets were made to a nominal grammage of 170 g/m^2 and a nominal apparent density of 600 kg/m^3. The morphology and orientation distribution of the fibers were measured microscopically in the dried sheets. The results were a mean fiber length of 2.2 mm, a mean fiber width of 30 μm, and a mean fiber thickness of 8 μm. A value of $a_1 = 0.0$ in Eq. (3) was found to represent the experimental uniform fiber orientation distribution while $a_1 = 0.79$ was found to represent that for the non-uniform orientation sheets.

Simple tension experiments were performed. In order to inhibit tension buckling (Seo et al., 1992), a neck down sample geometry was used with a gage section length of 76 mm and width of 19 mm along with a shoulder to gage section width ratio of 2.0. An extensometer was used to measure strain and the tests were performed using a nominal strain rate of 0.001 s^{-1}. Due to inherent variability, several tests were performed for each material set.

During testing it was observed that the majority of the tension samples failed along a localized deformation zone formed at a distinct orientation with respect to the transverse-to-loading direction. A photograph of such a failure zone is given in Fig. 4. In order to quantify the orientation of failure (since not all

Fig. 4. Example of a localized failure zone in a sample with $a_1 = 0.0$. The high level of fiber pull-out is apparent.

samples failed along a continuous line), expanded images of the failed tension samples were made and placed on a digitizing table. The profile length of each failure zone l_{fz}, was measured and the orientation angle ϕ_{fz}, was determined using the following relationship for gage section width w,

$$\phi_{fz} = \cos^{-1}\left(\frac{w}{l_{fz}}\right). \tag{18}$$

Note that the angle ϕ_{fz} was measured from the horizontal lines drawn on the sample in Fig. 4.

4. Results

Mean simple tension results are given in Fig. 5 for both the $a_1 = 0.0$ and $a_1 = 0.79$ fiber orientation sheet sets. The density of the $a_1 = 0.0$ network models were made equal to the density of the laboratory material as per Eqs. (4) and (5). The total number of bonds in the $a_1 = 0.79$ networks was then made equal to the mean number of bonds in the $a_1 = 0.0$ networks. This point will be commented on later. Fiber material parameters were determined by matching the simulation results to the experimental curves for the $a_1 = 0.79$ material. These network structure and material parameters are given in Table 1. Uniform ($a_1 = 0.0$) orientation simulations were then performed using these parameters. Twelve simulations were performed for each material set. The mean results are compared against the experimental results in Fig. 5. It is important to note that an isotropic representation of the plastic response of the fiber, i.e. $\alpha^0 = 0$; could not adequately describe the experimental data. The material parameters given in Table 1 correspond to a yield stress in tension of 250 MPa and that in compression of 50 MPa. Mechanistically the lower compressive yield stress is believed to represent inelastic buckling of the fiber segments. This general observation of in situ fiber behavior has also been made by Ramasubramanian and Perkins (1988).

Results of the localized failure zone orientation measurements are given in Table 2. The first principal material direction is the manufactured direction (MD) while the second principal direction is perpendicular to the manufactured direction (CD). Observations made during tension testing show that significant shear deformation occurred in the localized zone and along the line of localization after initiation. Ranger and Hopkins (1962) suggest that failure of fiber segments loaded in compression during simple tension loading

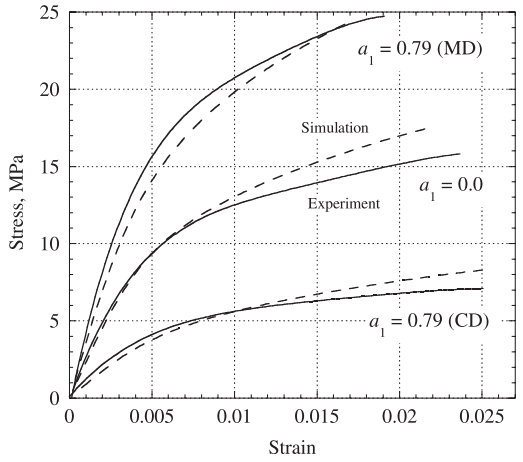

Fig. 5. Comparison between simple tension experimental data and simulation results. Each experimental curve represents the average of at least five tests. Each simulation curve is the average of twelve simulations. The manufactured direction is designated by MD and the cross-direction by CD.

Table 1
Material and network properties used for the monotonic and cyclic simple tension models

Loading	E_f (GPa)	v	σ^0 (MPa)	α^0 (MPa)	C (MPa)	l_f (mm)	a_1
Monotonic	48	0.3	150	100	725	2.2	0.0, 0.79
Cyclic	33	0.3	99	66	200	2.2	0.0

Table 2
Mean localized tensile failure zone orientation angles along with standard deviations for experiments, ϕ_{fz} and numerical simulations, θ_{zs}. The angles are measured from a line perpendicular to the tensile loading direction, shown in Fig. 4. The parameter a_1 defines the fiber orientation distribution in Eq. (3). MD indicates manufactured (machine) direction and CD cross direction

	$a_1 = 0.0$	$a_1 = 0.79 - \text{MD}$	$a_1 = 0.79 - \text{CD}$
Experimental, ϕ_{fz}	$37.5° \pm 6.8°$	$50.1° \pm 7.9°$	$24.0° \pm 3.7°$
No. of samples	28	28	12
Simulation, θ_{zs}	$30.2° \pm 0.6°$	$38.1° \pm 0.6°$	$25.3° \pm 0.7°$

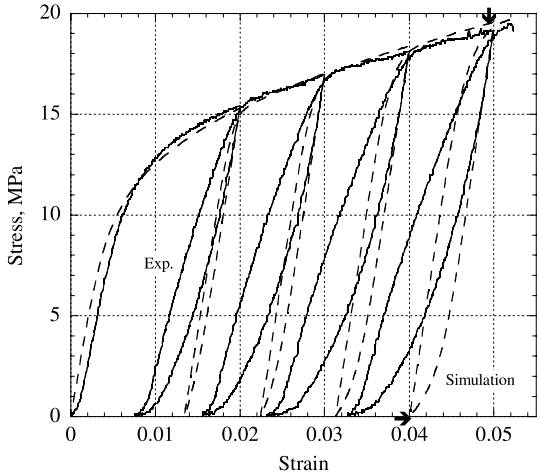

Fig. 6. Comparison between cyclic tension experimental data and simulation results. Each of the curves represents a single test and simulation. The arrows indicate the point in the deformation history where Fig. 7a (upper arrow) and b (lower arrow) were taken.

is responsible for strain-line formation. Strain lines are small pre-failure localization zones visually observed in some paper materials (Korteoja et al., 1996). It is unknown if strain lines are related to the formation of localized failure zones. Ranger and Hopkins (1962) presented a simple energy minimization model to describe this localization by assuming that fiber segments were linear elastic and unable to support compressive load. An attempt was made here to use the Ranger and Hopkins model with an anisotropic elastic–plastic constitutive model for the fiber to predict the localized failure zone angles in Table 2. The results gave unrealistically small angle magnitudes and are not reported here.

For polycrystalline metal samples of similar geometry, oblique necking frequently occurs. Hill (1950) proposed that the inclination of the necked zone to the transverse-to-loading direction is the same as that of a material line of zero extension. Using Hill's concept, the direction of zero extension in the tension network models was determined at the maximum strain for each simulation (0.022 for $a_1 = 0.0$, 0.017 for $a_1 = 0.79$ MD, 0.025 for $a_1 = 0.79$ CD). This was done by plotting the beam center line stress (normal component) versus beam segment angle. This information was then fit to a sinusoidal function and the angle of zero

stress, θ_{zs}, determined relative to the transverse-to-loading direction. These results are compared against those of the experiments in Table 2. As the statistics show, the localization behavior is highly variable.

One cyclic tension experiment was performed. The wood species used to make the laboratory material for this measurement was different from that used for the monotonic tests, although both were unrefined bleached Kraft pulps with similar mean fiber length. Material parameters were determined by matching the simulation to the upper loading portion of the cyclic tension curve. The parameter α^0 was chosen to give the same initial tension/compression yield ratio as used for the monotonic tension results given in Fig. 5. These network and material parameters are given in Table 1. Only one simulation and experiment were performed and are given in Fig. 6. The initial slope of the unloading curves matches that of the model, suggesting that significant interfiber bond failure has not occurred in the material. Qualitatively the model does well in representing the experimental results. The discrepancy in the latter stages of unloading is speculated to be due to time-dependent strain recovery of the material which is not represented by the time-independent fiber constitutive model.

5. Discussion

Through the use of the stochastic multi-scale modelling approach presented here, we are allowed the opportunity to observe the evolution of complex internal stress states during deformation. Fig. 7 gives the beam center-line normal stress of all the segments within the model used for cyclic tension. Fig. 7a corresponds to a point in the deformation history where the loading cycle terminates at a strain of 0.05. This point is indicated by the upper arrow in Fig. 6. The loading direction is at $\pm 90°$. A sinusoidal function is fit to the data and is also shown. Fig. 7a shows that in addition to tension yielded segments, a significant number of segments have yielded in compression—primarily those within 30° of the transverse-to-loading direction. Recall that differential tension and compression behavior was necessary to adequately represent the simple tension data. Mechanistically this is thought to represent the buckling of those fiber segments

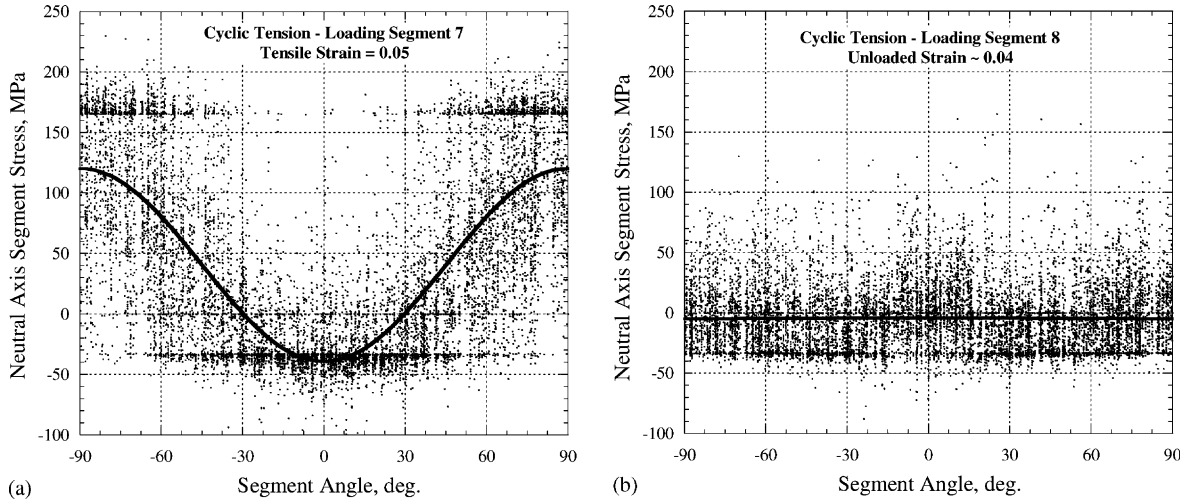

Fig. 7. Distribution of center-line stress in the beam segments of the network used to simulate cyclic tension. The location in the deformation history where each plot was taken is given in Fig. 6, (a) loaded—upper arrow, (b) unloaded—lower arrow. Segment angle is the orientation of the fiber segment relative to the transverse-to-loading direction.

loaded in compression. This is also consistent with the well observed difference between tension and compression behavior of paper in general (e.g. Bronkhorst and Bennett, 2001; Xia et al., 2002).

The wide distribution in stress at a given segment orientation angle is also apparent in Fig. 7. This is because each fiber must have zero stress at its ends and on average maximum stress near its center. In addition, the range of stress within a fiber is also a function of its neighborhood, not simply its orientation with respect to the loading direction. Fig. 7b corresponds to the internal stress state at an unloaded strain of 0.04 as indicated by the lower arrow in Fig. 6. This represents a state of residual stress. The non-linear unload curves of the model are a result of compression yielded beam segments. There appear to be two broad zones of compression yielded beam segments centered around $\pm 45°$. A sinusoidal function is fit to the data and is also shown in Fig. 7b. The resulting horizontal line falls at approximately 5 MPa. Note that bending and elastic shear stresses are not represented in the figure.

If one compares the numerical representation of the fibers used here to experimental results of single wood pulp fibers deformed in tension (e.g. Page and El-Hosseiny, 1983) it is found that the Young's moduli compare reasonably well but the model fiber tangent modulus is significantly smaller than experimental results would recommend (Fig. 8). It is reasonable to say that the model does not capture sufficient inelastic compliance. At the outset one must begin by considering the fiber mass which directly participates in interfiber bonding. Although not well understood, it is believed that during the drying of paper, fibers change dimension at the interfiber bond sites in a way which causes the fibers to form microcompressions or a saddle-shaped interface surface (Retulainen et al., 1998). It is certainly known that preventing shrinkage during drying decreases the elastic compliance of paper as shown in Fig. 9. Perhaps the inelastic compliance of this bond zone material is different from fiber segments which do not participate directly in interfiber bonding. The possibility for this difference was acknowledged in the micromechanics formulation offered by Ramasubramanian and Perkins (1988) and Sinha and Perkins (1995). The difficulty comes in quantifying the in situ deformation behavior within the two regions. It would seem that one would need to supplement macroscopic deformation experiments with those performed on single fibers. In addition, interfiber bonded fiber segments experience something closer to shear loading rather than simple tension.

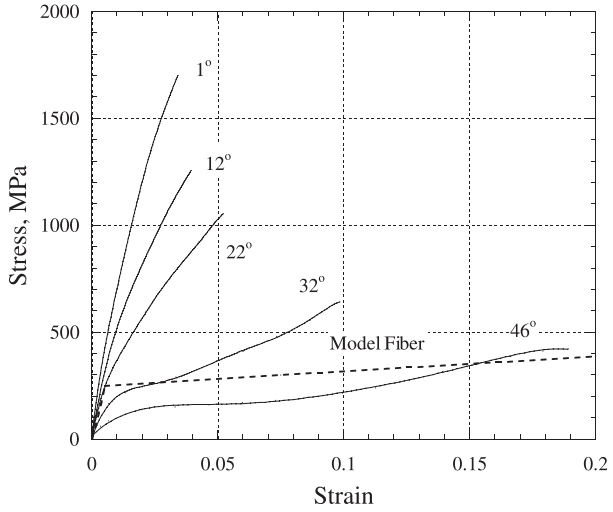

Fig. 8. Comparison between the tensile stress–strain response of wood pulp fibers (Page and El-Hosseiny, 1983) and the tensile stress–strain curve used for the fiber in the network model (Table 1, monotonic case). The angle value marking each experimental curve represents the mean S_2 layer microfibril angle of the fibers used for the experiments.

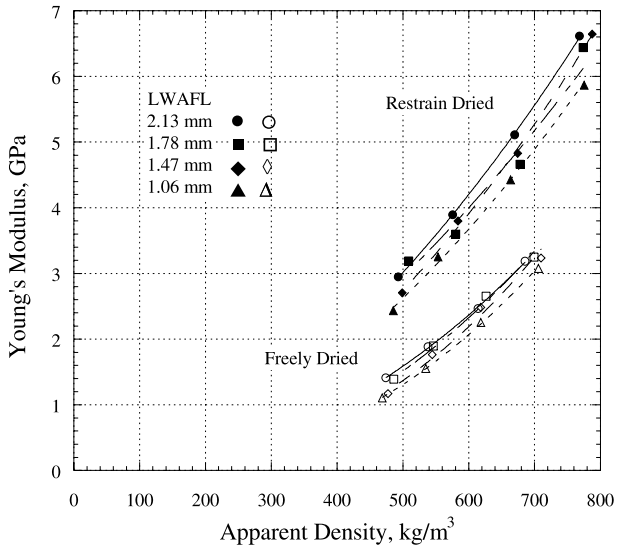

Fig. 9. Experimental data showing the effect of fiber length on Young's modulus for bleached Kraft pulp laboratory material. The upper sets of curves are for materials which were prevented from shrinking in the plane during drying. The lower curves are for those allowed to freely shrink.

Fig. 10 gives simulation results showing the elastic behavior of $a_1 = 0.0$ networks as a function of fiber length. The Young's modulus and Poisson ratio used for the fibers in the models were 48 GPa and 0.3 respectively. It is striking how large the impact of fiber length is on the Young's modulus of the numerical

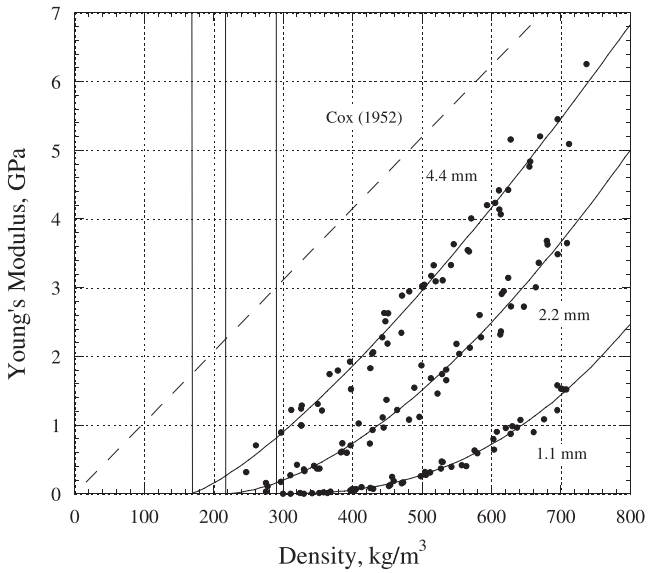

Fig. 10. Simulated Young's modulus versus density for three different constant fiber lengths used to form the networks: 1.1, 2.2 and 4.4 mm. A single fiber Young's modulus, $E_f = 48$ GPa and Poisson ratio, $\nu_f = 0.3$ were used. The upper broken line is the relationship suggested by Cox (1952).

sheets. As Eq. (6) suggests and the network models confirm, this is not a result of differences in interfiber contact. The reason for the results of Fig. 10 must therefore be one of network connectivity. Note that each fiber length (relative to the size of the network) has a different percolation threshold −164 kg/m^3 at 4.4 mm fiber length, 216 kg/m^3 at 2.2 mm, and 286 kg/m^3 at 1.1 mm. The relationship suggested by Cox (1952) is also plotted in Fig. 10. In Cox's analytical model the fibers are infinitely long and not bonded to each other. The Cox relationship is

$$E_s = \frac{1}{3}\frac{\rho_s}{\rho_f}E_f \tag{19}$$

where E_f is the fiber Young's modulus, ρ_s is the sheet density and ρ_f the fiber density. The curves appear to approach that of Cox as the fibers get long. The Cox model is not a rigid network however (Ostoja-Starzewski and Stahl, 2000). It is also not clear that the Young's modulus differences due to percolation are ever eliminated at greater coverage in the case of a two-dimensional model. For some perspective, Young's modulus versus apparent density data for bleached Kraft pulp handsheets is given in Fig. 9. The simulation results suggest a greater sensitivity to fiber length than the experimental data shows. This clearly points out a short-coming of a two-dimensional representation of paper. Each two-dimensional fiber network is essentially a single fiber layer within a sheet of paper. In the current model, a single fiber is connected only to other fibers within this single layer. In paper, a fiber is believed to not only be connected to fibers within its own layer but also to fibers in adjacent layers (Kallmes et al., 1961). This would then suggest that a two-dimensional representation significantly under-represents the true level of connectivity existing in paper—a three-dimensional fibrous network. Early attempts (Heyden and Gustafsson, 2001; Stålne and Gustafsson, 2001) at three-dimensional models demonstrate the difficulty in doing so for these orthotropic disordered materials.

Results suggest that the mass of material participating directly in interfiber bonding must be explicitly accounted for. In the present concept, each fiber crossing is considered as a dimensionless rigid bond between beam elements. In this case as fiber orientation is increased, the number of interfiber contacts decreases (Eq. (6)). This is the reason for matching the total number of fiber bonds for the $a_1 = 0.79$ models to that for the $a_1 = 0.0$ models discussed earlier. However for fibers of finite width as fiber orientation is

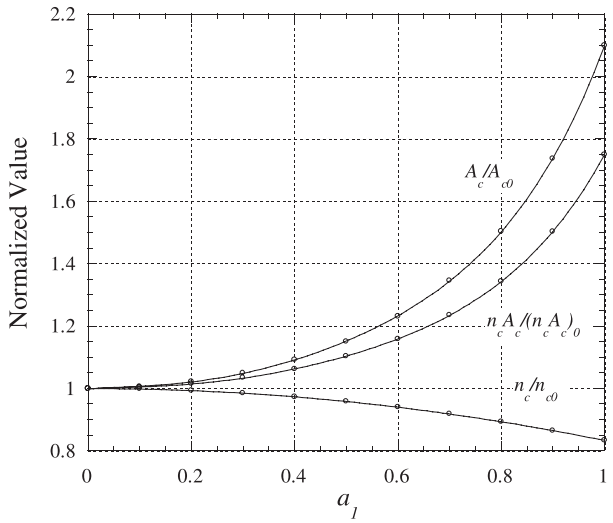

Fig. 11. Evolution of the two-dimensional network bonding state with fiber orientation parameter a_1 when accounting for fibers of finite width.

increased so too does the mean area per fiber crossing (Eq. (8)). The product of these two equations must be represented in the model. Eqs. (6) and (8) along with their product is shown in Fig. 11.

In his mesoscopic view of paper, Perkins (1980) used the work of Komori and Makishima (1977) to link distance between interfiber bonds along a fiber to sheet density as a way to represent the density of the three-dimensional material. In doing so the following relationship was used

$$\bar{l}_{3D} = \frac{\pi \rho_f w_f}{4\rho_s\left(1 - \frac{\pi}{6}a_1^2\right)} \tag{20}$$

If we equate Eqs. (7) and (20) we see that there is a critical coverage $\bar{c}_{cr}$, which the two-dimensional network must attain in order to achieve the level of interfiber bond distance given by Eq. (20).

$$\bar{c}_{cr}(1 + \exp(-\bar{c}_{cr})) = 8\frac{\rho_s}{\rho_f}\frac{6 - \pi a_1^2}{6 - a_1^2} \tag{21}$$

If we use typical values for the parameters in Eq. (21) ($\rho_s = 600$ kg/m^3, $\rho_f = 1540$ kg/m^3, $a_1 = 0.6$) we get a critical coverage of 2.5 (compared to $\bar{c} \cong 0.4$ networks used here). This result suggests that even if sheets are at equivalent apparent densities, those which do not have a grammage which is greater than some critical value will behave differently.

6. Conclusion

This work should be viewed as a first-order attempt at comprehensively describing the stochastic multi-scale inelastic behavior or paper. The simple model approach presented does a reasonable job representing the simple tension data. Certainly more work is needed however. Although especially true at smaller size scales, we must also include the third dimension in our representation. Without doing so it is impossible to decouple network grammage from network density. Interfiber bonding must also be more adequately represented for its potential impact on the inelastic response of these fiber systems.

Acknowledgements

The experimental assistance of T. Duong and J.R. Riedemann is gratefully acknowledged.

References

ABAQUS, 1998. version 5.8, Hibbitt, Karlsson & Sorenson, Pawtucket RI.

Åström, J., Saarinen, S., Niskanen, K., Kurkijarvi, J., 1994. Microscopic mechanics of fiber networks. Journal of Applied Physics 75 (5), 2383–2392.

Bronkhorst, C.A., Bennett, K.A., 2001. Deformation and failure behavior of paper. In: Mark, R.E., Habeger, C.C., Borch, J., Lyne, M.B. (Eds.), Handbook of Physical Testing of Paper, vol. 1. Marcel Dekker, New York, pp. 313–427.

Corte, H., 1971. Statistical geometry of random fibre networks. In: Te'eni, M. (Ed.), Structure, Solid Mechanics and Engineering Design: The Proceedings of the Southhamptom 1969 Civil Engineering Materials Conference. Wiley-Interscience, pp. 341–355.

Cox, H.L., 1952. The elasticity and strength of paper and other fibrous materials. British Journal of Applied Physics 3 (3), 72–79.

Deng, M., Dodson, C.T.J., 1994. Paper: An Engineered Stochastic Structure. TAPPI Press, Atlanta. p. 88.

Heyden, S., Gustafsson, P.J., 1998. Simulation of fracture in a cellulose fibre network. Journal of Pulp and Paper Science 24 (5), 160–165.

Heyden, S., Gustafsson, P.J., 2001. Stress–strain performance of paper and fluff by network modelling. In: Baker, C.F. (Ed.), The Science of Papermaking. The Pulp & Paper Fundamental Research Society, Lancashire, UK, pp. 1385–1401.

Hill, R., 1950. The Mechanical Theory of Plasticity. Oxford University Press, London. p. 356.

Kallmes, O., Corte, H., Bernier, G., 1961. The structure of paper II. The statistical geometry of a multiplanar fiber network. Tappi Journal 44 (7), 519–528.

Komori, T., Makishima, K., 1977. Numbers of fiber-to-fiber contacts in general fiber assemblies. Textile Research Journal 47 (1), 13–17.

Korteoja, M.J., Lukkarinen, A., Kaski, K., Gunderson, D.E., Dahlke, J.L., Niskanen, K.J., 1996. Local strain fields in paper. Tappi Journal 79 (4), 217–223.

Mark, R.E., 2001. Mechanical properties of fibers. In: Mark, R.E., Habeger, C.C., Borch, J., Lyne, M.B. (Eds.), Handbook of Physical Testing of Paper, vol. 1. Marcel Dekker, New York, pp. 727–872.

Ostoja-Starzewski, M., 1998. Random field models of heterogeneous materials. International Journal of Solids and Structures 35 (19), 2429–2455.

Ostoja-Starzewski, M., Stahl, D.C., 2000. Random fiber networks and special elastic orthotropy of paper. Journal of Elasticity 60, 131–149.

Page, D.H., El-Hosseiny, F., 1983. The mechanical properties of single wood pulp fibres, Part IV, fibril angle and the shape of the stress–strain curve. Journal of Pulp and Paper Science 9 (4), 1–2.

Perkins, R.W., 1980. Mechanical behavior of paper in relation to its structure. In: Proceedings of Paper Science and Technology—The Cutting Edge. The Institute of Paper Chemistry, Appleton, WI, pp. 89–111.

Perkins, R.W., 2001. Models for describing the elastic, viscoelastic, and inelastic mechanical behavior of paper and board. In: Mark, R.E., Habeger, C.C., Borch, J., Lyne, M.B. (Eds.), Handbook of Physical Testing of Paper, vol. 1. Marcel Dekker, New York, pp. 1–76.

Perkins, R.W., Mark, R.E., 1976. On the structural theory of the elastic behavior of paper. Tappi Journal 59 (12), 118–120.

Räisänen, V.I., Alava, M.J., Nieminen, R.M., Niskanen, K.J., 1996. Elastic–plastic behaviour in fibre networks. Nordic Pulp and Paper Research Journal 11 (4), 243–248.

Ramasubramanian, M.K., Perkins, R.W., 1988. Computer simulation of the uniaxial elastic–plastic behavior of paper. Journal of Engineering Materials and Technology 110 (1), 117–123.

Ramasubramanian, M.K., Wang, Y.Y., 1999. Constitutive models for paper and other ribbon-like nonwovens—A literature review. In: Perkins, R. (Ed.), Mechanics of Cellulosic Materials, AMD-Vol. 231, MD-Vol. 85. American Society of Mechanical Engineers, New York, pp. 31–42.

Ranger, A.E., Hopkins, L.F., 1962. A new theory of the tensile behavior of paper. In: Bolam, F. (Ed.), Formation and Structure of Paper, vol. 1. Technical Section of the British Paper and Board Makers Association, London, pp. 277–310.

Retulainen, E., Niskanen, K., Nilsen, N., 1998. Fibers and bonds. In: Niskanen, K. (Ed.), Paper Physics. Finnish Paper Engineers' Association, Helsinki and TAPPI Press, Atlanta, pp. 54–87.

Seo, Y.B., Chaves de Oliveira, R., Mark, R.E., 1992. Tension buckling behaviour of paper. Journal of Pulp and Paper Science 18 (2), 55–59.

Sinha, S.K., Perkins, R.W., 1995. A micromechanics constitutive model for use in finite element analysis. In: Mechanics of Cellulosic Materials, AMD-Vol. 209/MD-Vol. 60. American Society of Mechanical Engineers, New York.

Stålne, K., Gustafsson, P.J., 2001. A three dimensional finite element fibre network model for composite material stiffness and hygroexpansion analysis. Proceedings of the European Conference on Computational Mechanics. 26–29 June, Cracow, Poland.

Van den Akker, J.A., 1962. Some theoretical considerations on the mechanical properties of fibrous structures. In: Bolam, F. (Ed.), The Formation and Structure of Paper. Technical Section British Paper and Board Makers Association, London, pp. 205–241.

Wang, Y.Y., 2000. Constitutive Modeling of the Unloading Behavior of Paper Material Using the Asymptotic Fiber and Bond Model, Ph.D. Thesis, North Carolina State University.

Xia, Q.S., Boyce, M.C., Parks, D.M., 2002. A constitutive model for the anisotropic elastic–plastic deformation of paper and paperboard. International Journal of Solids and Structures 39 (15), 4053–4071.